The structural connectome constrains fast brain dynamics

Supplementary Material

Sorrentino P[1,2^], Seguin C[3], Rucco R[4,5], Liparoti M[4,5], Troisi Lopez E[4,5], Bonavita S[6], Quarantelli M[7], Sorrentino G[4,5], Jirsa V[1*]& Zalesky A[3*]

* Co-senior authors

^ Corresponding author: pierpaolo.SORRENTINO@univ-amu.fr

1. **Institut de Neurosciences des Systèmes, Aix-Marseille University, Marseille, France**
2. **Institute of Applied Sciences and Intelligent Systems, National Research Council, Pozzuoli, Italy**
3. **University of Melbourne, Melbourne, Australia**
4. **Department of Motor Sciences and Wellness, Parthenope University of Naples, Naples, Italy**
5. **Institute for Diagnosis and Cure Hermitage Capodimonte, Naples, Italy**
6. **University of Campania Luigi Vanvitelli. Caserta, Italy**
7. **Biostructure and Bioimaging Institute, National Research Council, Naples, Italy**

Materials and Methods

2.1 Participants

We initially enrolled 58 young adults (male 32 / female 26, mean age ± SD was 30.72 ± 11.58). All participants were right-handed and native Italian speakers. The inclusion criteria were: 1) no major internal, neurological or psychiatric illnesses; 2) no use of drugs or medication that could interfere with MEG/MRI signals. The study complied with the Declaration of Helsinki and was approved by the local Ethics Committee. All participants gave written informed consent.

2.2 MRI acquisition

3D T1-weighted brain volumes were acquired at 1.5 Tesla (Signa, GE Healthcare) using a 3D Magnetization-Prepared Gradient-Echo BRAVO sequence (TR/TE/TI 8.2/3.1/450 ms, voxel 1 × 1 × 1 mm3, 50% partition overlap, 324 sagittal slices covering the whole brain). The MRI scan was performed after the MEG recording.

2.3 Tractography analysis

A subject-specific connectome was obtained in all subjects on the same MRI scanner (1.5 Tesla, Signa, GE Healthcare). DTI preprocessing was carried out using the software modules provided in the FMRIB Software Library (FSL, http://fsl.fmrib.ox.ac.uk/fsl). All DTI datasets were corrected for head movements and eddy currents distortions using the "eddy_correct" routine, rotating diffusion sensitizing gradient directions accordingly, and a brain mask was obtained from the B0 images using the Brain Extraction Tool routine. A diffusion-tensor model was fitted at each voxel, and fiber tracks were generated over the whole brain by deterministic tractography using Diffusion Toolkit (FACT propagation algorithm, angle threshold 45°, spline-filtered, masking by the FA maps thresholded at 0.2). For tractographic analysis, the ROIs of the AAL atlas and of a MNI space-defined volumetric version of the Desikan-Killiany-Tourville (DKT) ROI atlas were used, both masked by the GM tissue probability map

available in SPM (thresholded at 0.2). To this end, for each participant, FA volumes were normalized to the MNI space using the FA template provided by FSL, using the spatial normalization routine available in SPM12, and the resulting normalization matrices were inverted and applied to the ROIs, to apply them onto each subject. The quality of the normalization was assessed visually. From each subject's whole brain tractography and corresponding GM ROI set, the number of streamlines connecting each couple of GM ROIs and the corresponding mean tract length was calculated using an in-house software written in Interactive Data Language (IDL, Harris Geospatial Solutions, Inc., Broomfield, CO, USA).
Connectomes in the replication dataset were constructed using an alternative mapping pipeline and high-quality diffusion MRI data from the Human Connectome Project (HCP). Deterministic tractography was performed using MRtrix3 (1) under the following parameters: FACT algorithm, 5 million streamlines, 0.5 mm propagation step size, 400 mm maximum propagation length, and 0.1 FA threshold for the termination of streamlines (2)Structural matrices were constructed 200 HCP participants using the AAL atlas and averaged to derive a group-level connectome.

2.5 Acquisition

The data were acquired using a MEG system equipped by 154 magnetometers (SQUID - Superconducting Quantum Interference Device) placed as close as possible to the head of the subjects, and 9 references sensors in order to record the environmental noise (3). The system is placed in a magnetically shielded room (AtB Biomag, Ulm, Germany) to reduce the external noise. The MEG registration was split into two eyes-close segment of 3 minute and half. To identify the right position of the head within the helmet, before each recording, the position of four anatomical points (nasion, right and left pre-auricular points and vertex of the head) and four coils (two attached on the forehead, one behind the right ear and one behind the left ear) were digitized by using Fastrak (Polhemus®). The coils were activated at the beginning of each segment of the registration. Electrocardiogram (ECG) and electro-oculogram (EOG) were also recorded during the acquisition (4).

2.6 Preprocessing

The MEG signals, after an anti-aliasing filter, were acquired at 1024 Hz, then a fourth order Butterworth IIR band-pass filter in the 0.5-48 Hz band was applied (5). To remove the environmental noise, measured by reference magnetometers, we used Principal Component Analysis (6), while we adopted Independent Component Analysis (7) to clean the data from physiological artifacts, such as eye blinking (if present) and heart activity (generally one component). Noisy channels were identified and removed manually by an expert rater (8). 47 subjects had enough clean data and were selected for further analysis.

2.7 Source reconstruction

The time series of neuronal activity were reconstructed in 116 regions of interests (ROIs) based on the Automated Anatomical Labeling (AAL) atlas (9, 10); and in 84 regions of interest based on the Desikan-Killiany-Tourreville (DKT) atlases. To do this, we used the volume conduction model proposed by Nolte (11) applying the Linearly Constrained Minimum Variance (LCMV) beamformer algorithm (12) based on the native MRIs. Sources were reconstructed for the centroids of the each ROI. Finally, we considered a total of 90 ROIs since we have excluded 26 ROIs corresponding to the cerebellum because of their low reliability in MEG (13). All the preprocessing steps and the source reconstruction are made using the Fieldtrip toolbox (14).

2.8 Neuronal avalanches and branching parameter

To study the dynamics of brain activity, we estimated "neuronal avalanches". Firstly, the time series of each ROI was discretized calculating the z-score, then positive and negative excursions beyond a threshold were identified. The value of the threshold was set to 3 standard deviations ($|z| = 3$), but we tested the robustness of the results changing this threshold from 2.5 to 3.5. A neuronal avalanche begins when, in a sequence of contiguous time bins, at least one ROI is active ($|z| > 3$), and ends when all ROIs are inactive (15, 16). The total number of active ROIs in an avalanche corresponds to its size.

These analyses require the time series to be binned. This is done to ensure that one is capturing critical dynamics, if this is present. To estimate the suitable time bin length, for each subject, for each neuronal avalanches and for each time bin duration, the branching parameter σ was estimated (17, 18). In fact, system operating at criticality typically display a branching ratio ~1. The branching ratio is calculated as the geometrically averaged (over all the time bins) ratio of the number of events (activations) between the subsequent time bin (descendants) and that in the current time bin (ancestors) and then averaging it over all the avalanches (19). More specifically:

$$\sigma_i = \frac{1}{N_{bin}-1} \prod_{j=1}^{N_{bin}-1} \left(\frac{n_{events}\,(j+1)}{n_{events}\,(j)} \right)^{\frac{1}{N_{bin}-1}} \quad (1)$$

$$\sigma = \frac{1}{N_{aval}} \prod_{i=1}^{N_{aval}} (\sigma_i)^{\frac{1}{N_{aval}}} \quad (2)$$

Where σ_i is the branching parameter of i-th avalanche in the dataset, N_{bin} is the total amount of bins in the i-th avalanche, $n_{events}\,(j)$ is the total number of events active in the j-th bin, N_{aval} is the total number of avalanche in the dataset. We tested bins from 1 to 5, and picked 3 for further analyses, given that the branching ratio was 1 for bin =3. However, results are unchanged for other bin durations (data not shown). The results shown are derived when taking into accounts avalanches longer than 10 time bins. However, we repeated the analysis taking into account avalanches longer than 30 time bins, as well as taking all avalanches into account, and the results were unchanged.

2.9 Randomization procedure

To validate our results, we used a null model based on the assumption that the topological organization of the connectome does not affect the spreading of activations in time. Hence, every avalanche, for every subject, was randomized in time (i.e. the order of the time bins was reallocated randomly, while the spatial ordering of the activations (i.e. across regions) was left unchanged). A surrogate transition matrix was computed per each surrogate avalanche. These surrogate transition matrices were then averaged within each subject and then across subjects. The resulting group surrogate matrix was then symmetrized and compared to the structural connectome obtained as the average of the subject specific tractographies using Spearman rank correlation. The procedure described above was repeated a thousand time, retrieving a null distribution of r's and p's of the Spearman correlations. These distributions were then compared to the observed p and r.

Results

3.1 Alternative estimation of Transition Matrices.

To further rule out the possibility that the transition matrix is an effect of volume conduction, we built the transition matrix using an alternative procedure, which maximizes consecutive lags between consecutive activations. To this end we checked, once an avalanche started (i.e. some regions were above threshold), what other regions followed, regardless of the time lag. In other words, we did not scroll along the time of the avalanche to compute a probability of activation, but we simply noted what regions activated after the first perturbation. This way, the delays accounted for were up to the length of the avalanche itself. This procedure was carried out for the AAL atlas, in the case of binning =3, z-score threshold = ± 3.
As shown in Supplementary figure 1, we were able to replicate the results using this alternative procedure to map transition matrices, further suggesting that the impact of volume conduction is an unlikely confound.

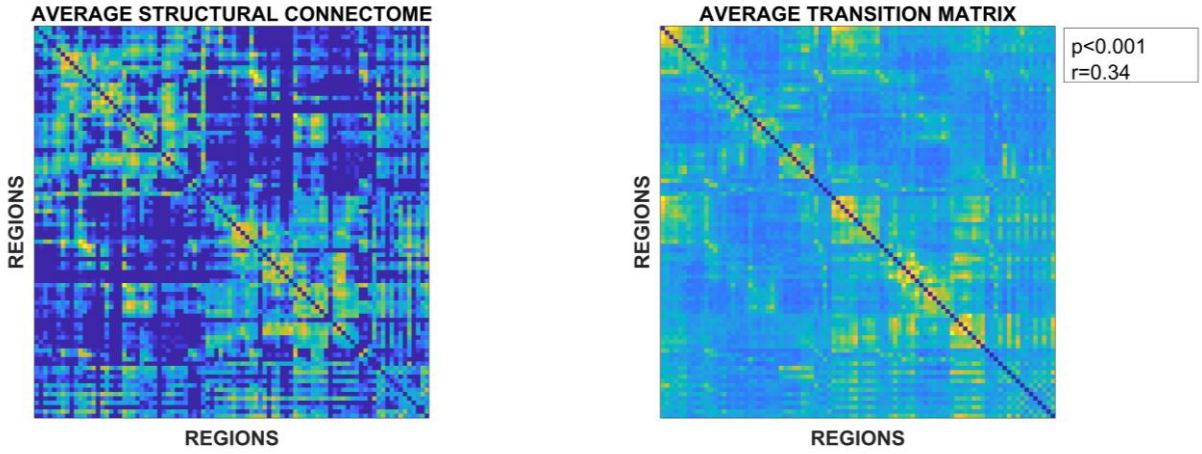

3.2 Frequency – specific analysis

To explore if any frequency-specific effect was evident, we carried out the analysis after filtering the reconstructed signals in the classical frequency bands: delta (0.5 – 4 Hz), theta (4 – 8 Hz), alpha (8 – 13 Hz), beta (13 – 30 Hz) and gamma (30 – 48 Hz). To this end, we applied a fourth-order Butterworth pass-band filter, before proceeding to the further analysis as previously described. The results remained significant in all the explored frequency bands. This analysis was carried out for the DKT atlas, binning = 3, z-score threshold = ± 3.

	R	p
Delta (0.5 – 4 Hz)	**0.39**	**2.07e-88**
Theta (4 – 8 Hz)	**0.29**	**4.95e-70**
Alpha (8 – 13 Hz)	**0.32**	**2.11e-84**
Beta (13 – 30 Hz)	**0.32**	**7.23e-88**
Gamma (30 – 48 Hz)	**0.32**	**3.84e-88**

References

1. J. D. Tournier, *et al.*, MRtrix3: A fast, flexible and open software framework for medical image processing and visualisation. *Neuroimage* **202**, 116137 (2019).
2. C. Seguin, A. Razi, A. Zalesky, Inferring neural signalling directionality from undirected structural connectomes. *Nat. Commun.* **10**, 1–13 (2019).
3. R. Rucco, *et al.*, Brain connectivity study by multichannel system based on superconducting quantum magnetic sensors. *Eng. Res. Express* **2** (2020).
4. P. Sorrentino, *et al.*, Brain functional networks become more connected as amyotrophic lateral sclerosis progresses: a source level magnetoencephalographic study. *NeuroImage Clin.* **20**, 564–571 (2018).
5. R. Rucco, *et al.*, Mutations in the SPAST gene causing hereditary spastic paraplegia are related to global topological alterations in brain functional networks. *Neurol. Sci.* **40**, 979–984 (2019).
6. D. N. P.K. Sadasivan, SVD based technique for noise reduction in electroencephalographic signals. *Signal Processing* **55**, 179–189 (1996).
7. G. Barbati, C. Porcaro, F. Zappasodi, P. M. Rossini, F. Tecchio, Optimization of an independent component analysis approach for artifact identification and removal in magnetoencephalographic signals. *Clin. Neurophysiol.* **115**, 1220–1232 (2004).
8. F. Jacini, *et al.*, Amnestic Mild Cognitive Impairment Is Associated With Frequency-Specific Brain Network Alterations in Temporal Poles. *Front. Aging Neurosci.* **10**, 400 (2018).
9. N. Tzourio-Mazoyer, *et al.*, Automated anatomical labeling of activations in SPM using a macroscopic anatomical parcellation of the MNI MRI single-subject brain. *Neuroimage* **15**, 273–89 (2002).
10. A. Hillebrand, *et al.*, Direction of information flow in large-scale resting-state networks is frequency-dependent. *Proc. Natl. Acad. Sci. U. S. A.* (2016) https:/doi.org/10.1073/pnas.1515657113.
11. G. Nolte, The magnetic lead field theorem in the quasi-static approximation and its use for magnetoencephalography forward calculation in realistic volume conductors. *Phys. Med. Biol.* **48**, 3637–3652 (2003).
12. B. D. Van Veen, W. Van Drongelen, M. Yuchtman, A. Suzuki, Localization of Brain Electrical Activity via Linearly Constrained Minimum Variance Spatial Filtering. *IEEE Trans. Biomed. Eng.* **44** (1997).
13. A. Lardone, *et al.*, Mindfulness meditation is related to long-lasting changes in hippocampal functional topology during resting state: a magnetoencephalography study. *Neural Plast.* **2018** (2018).
14. R. Oostenveld, *et al.*, FieldTrip: Open Source Software for Advanced Analysis of MEG, EEG, and Invasive Electrophysiological Data, FieldTrip: Open Source Software for Advanced Analysis of MEG, EEG, and Invasive Electrophysiological Data. *Comput. Intell. Neurosci.* (2011) https:/doi.org/10.1155/2011/156869, 10.1155/2011/156869.
15. J. M. Beggs, D. Plenz, Neuronal avalanches in neocortical circuits. *J. Neurosci.* **23**, 11167–77 (2003).
16. O. Shriki, *et al.*, Neuronal Avalanches in the Resting MEG of the Human Brain. *J. Neurosci.* **33**, 7079–7090 (2013).
17. C. Haldeman, J. M. Beggs, Critical Branching Captures Activity in Living Neural Networks and Maximizes the Number of Metastable States. *Phys. Rev. Lett.* **94**, 058101 (2005).
18. T. E. Harris, The Theory of Branching Process (1964).
19. P. Bak, C. Tang, K. Wiesenfeld, Self-organized criticality: An explanation of the 1/f noise. *Phys. Rev. Lett.* **59**, 381 (1987).